Journal of Molecular Liquids 168 (2012) 54–60

Contents lists available at SciVerse ScienceDirect

Journal of Molecular Liquids

journal homepage: www.elsevier.com/locate/molliq

Thermodynamic and dielectric spectroscopy of a racemic antiferroelectric liquid crystal

Suman Kumari [a,*], I.M.L. Das [a], R. Dhar [b], R. Dabrowski [c]

[a] Physics Department, University of Allahabad, Allahabad-211002, India
[b] Centre of Material Sciences, University of Allahabad, Allahabad-211002, India
[c] Institute of Chemistry, Military University of Technology, Warsaw 00-908, Poland

ARTICLE INFO

Article history:
Received 10 August 2011
Received in revised form 12 January 2012
Accepted 13 January 2012
Available online 3 February 2012

Keywords:
Dielectric spectroscopy
Liquid crystal
Relaxation
Antiferroelectric
Dielectric strength
Relaxation frequency

ABSTRACT

The thermodynamic and dielectric spectroscopy of a racemic antiferroelectric liquid crystal (R,S)-4′-(1-methylheptyloxycarbonyl)biphenyl-4-yl 4-[3-(2,2,3,3,4,4,4-heptafluorobutoxy)prop-1-oxy]-2,3-difluorobenzoate at room temperature is reported in this paper. On account of racemization, the material is composed of non chiral SmC and SmC_A phases instead of possessing the conventional chiral phases. Unlike the chiral SmC^* phase which shows the Goldstone mode during dielectric investigations, this material in the SmC phase has shown a Domain mode. This relaxation mode possesses weak dielectric strength and temperature dependent relaxation frequency. Two relaxation modes have been observed in the SmC_A phase. The dielectric strength of one of these modes is found to be almost temperature independent whereas that of the other is found to vary inversely with temperature. The relaxation frequencies of both of these relaxation modes have been examined to be directly related to the temperature.

1. Introduction

In the last two decades, a considerable number of theoretical and experimental works have been devoted to the study of dielectric and electro-optic properties of the ferro- and antiferro-electric liquid crystals (FLCs and AFLCs) [1–10]. Ferroelectricity in the chiral Smectic C (SmC^*) phase or ferroelectric (F) phase of liquid crystals (LCs) has been initially reported by Meyer et al. in 1975 [1]. However, antiferroelectricity in the chiral Smectic C_A (SmC^*_A) phase or antiferroelectric (AF) phase was first reported by Chandani et al. in 1989 [6]. In the SmC^* phase, molecules are tilted at an angle θ with respect to the smectic layer normal ($\hat{k}$). The molecules rotate through an azimuthal angle ϕ in the adjacent smectic layers and hence spontaneous polarization ($\bar{P}_S$) rotates from layer to layer forming a helical structure with $\hat{k}$ as the helix axis. This $\bar{P}_S$ is perpendicular to both the $\hat{k}$ and $\hat{c}$-directors. The SmC^*_A phase differs from the SmC^* phase in respect of orientation of molecules in adjacent smectic layers. In this phase, the molecules in neighboring layers are tilted in the opposite directions with respect to $\hat{k}$. Hence, the dipole moments of two adjacent layers are canceled out resulting in the zero net dipole moment. This implies the lack of macroscopic spontaneous polarization in the AF phase. Because of their specific molecular configuration and arrangement, the FLCs and AFLCs have shown great potential for their use in the electro-optical displays [2,5–8,10]. But, AFLCs are rather better over FLCs due to their tristate switching behavior (double hysteresis), easy DC compensation, microsecond response, hemispherical viewing angle, no ghost effect, gray scale capability and ability of multiplexing in passively addressed matrices [6–8,10]. To obtain quick electro-optic response necessary for their display applications, it is essential to first suppress helix of the F and AF phases of these materials. This situation can be achieved in the surface stabilized FLCs and AFLCs (SSFLCs and SSAFLCs) which are characterized by having the cell thickness less than the pitch of the material [11]. But it is difficult to manufacture cells of such small thickness and that too may be easily damaged from the mechanical shocks. The other method is to apply electric field to the helical states of these materials to unwind their helices. This requires a critical external electric field beyond which the alignment is destroyed. Moreover, such thin cells may not withstand the higher applied voltages. One of the methods to overcome these difficulties is to make a mixture of the R and S enantiomers of the AFLC material in the ratio 1:1, i.e., to make a racemic AFLC material. In this situation, $\bar{P}_S$ of the two enantiomers being in opposite directions, are canceled out due to the opposite optical rotation of their molecules. And thus, the helix does not exist in the racemic materials. This property will be helpful in the fast switching performance of these materials. Moreover, these racemic AFLCs are advantageous from the point of view of the alignment because it is very difficult to align chiral phases.

---

* Corresponding author. Present address: Government Polytechnic, Mirzapur-231001, U. P., India. Tel./fax: +91 532 2460993, +919452139007 (mobile).
E-mail addresses: suman2301@gmail.com, suman_2301@rediffmail.com (S. Kumari).

0167-7322/$ – see front matter © 2012 Elsevier B.V. All rights reserved.
doi:10.1016/j.molliq.2012.01.010

The aim of this work is to investigate the transition temperatures and the dielectric parameters viz. dielectric strength ($\Delta\varepsilon$) and relaxation frequency (f_R) of the various relaxation modes of a racemic AFLC material (R,S)-4′-(1-methylheptyloxycarbonyl)biphenyl-4-yl 4-[3-(2,2,3,3,4,4,4-heptafluorobutoxy)prop-1-oxy]-2,3-difluorobenzoate for which the ratio of R and S enantiomers, i.e., R:S is 1:1. The material was synthesized by Dabrowski's group (Institute of Chemistry, Military University of Technology, Warsaw 00-908, (Poland)). The molecular structure of the material is given below:

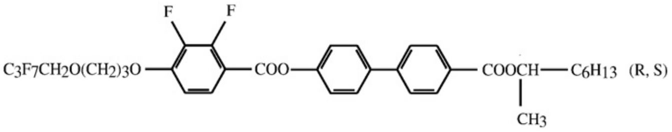

2. Experimental techniques

The phase transition temperatures and corresponding transition enthalpies have been obtained by Differential Scanning Calorimeter (DSC) of NETZSCH (model DSC 200F3 Maia). Peak transition temperatures (Tp) were determined to an accuracy of ±0.1 °C for fully grown peaks. However, for very weak peaks, uncertainties were large.

The different mesophases of the material have been identified during cooling by placing 10 μm thick planar aligned cell of the ITO coated glass plates under an optical polarizing microscope CENSICO (model IZUMI 7626).

The dielectric investigations have been carried out using planar aligned capacitor cell having electrodes made of ITO coated glass plates of sheet resistance 25 Ω/□ and WAT made gold coated cells. The spacing between the electrodes for ITO cell is 10 μm and that for the gold coated cell is 8.7 μm. The gold-coated electrodes give spontaneous planar alignment (long axes of the molecules are parallel to the plates and perpendicular to the applied field). The active capacitance (C_L) was determined by introducing an organic liquid of known dielectric constant (in this case cyclohexane) into the cell. Dielectric data were acquired by using a Hewlett–Packard impedance analyzer (model HP4194A) and impedance/gain-phase analyzer Solartron (model SI–1260) coupled with Solartron dielectric interface (model–1296) in the frequency range 0.1 Hz–10 MHz. The optical studies were carried out using the ITO electrode cells. The temperature of the sample for the optical and dielectric studies has been controlled by a hot stage (Instec-HS-1) with an accuracy of ±0.1 °C and the resolution limit of ±0.003 °C. The temperature near the sample has been determined by measuring thermo-emf of a copper-constantan thermocouple with the help of a six and half digit multimeter. Dielectric data have been acquired during the cooling cycle with a probing electric field of 500 mVrms. The acquired data of capacitance (C) parallel to the conductance (G) were used to determine the frequency dependent relative dielectric permittivity (ε') and dielectric loss (ε'') [12]. C and G were determined with a basic accuracy of 0.2%, and hence the maximum uncertainties in the determination of ε' and ε'' are not more than 1%. The accuracy of measured frequency is ±100 ppm. The dielectric data at 1 kHz have been taken as the 'static' values, as they are free from low and high frequency parasitic effects [13–15].

To analyze the measured data, the dielectric spectra have been fitted with the generalized Cole–Cole equation [16,17]

$$\varepsilon^{*}=\varepsilon^{'}-j\varepsilon^{''}=\varepsilon^{'}(\infty)+\sum_{i}\frac{(\Delta\varepsilon)_i}{1+\left(j\left(f/f_{R_i}\right)\right)^{(1-h_i)}}+\frac{A}{f^n}-j\frac{\sigma_{ion}}{2\pi\varepsilon_0 f^k}-jBf^m. \tag{1}$$

Real and imaginary parts of Eq. (1) can be written as

$$\varepsilon^{'}=\varepsilon^{'}(\infty)+\sum_{i}\Delta\varepsilon_i\frac{\left[1+\left(f/f_{R_i}\right)^{(1-h_i)}\sin(h_i\pi/2)\right]}{1+\left(f/f_{R_i}\right)^{2(1-h_i)}+2\left(f/f_{R_i}\right)^{(1-h_i)}\sin(h_i\pi/2)}+\frac{A}{f^n} \tag{2}$$

and

$$\varepsilon^{''}=\sum_{\mathrm{i}}\Delta\varepsilon_{\mathrm{i}}\frac{\left(f/f_{R_i}\right)^{(1-h_i)}\cos(h_i\pi/2)}{1+(f/f_{Ri})^{2(1-h_i)}+2\left(f/f_{R_i}\right)^{(1-h_i)}\sin(h_i\pi/2)}+\frac{\sigma}{2\pi\varepsilon_0 f^k}+Bf^m \tag{3}$$

where, $\Delta\varepsilon_i$ [$=\varepsilon'(0)-\varepsilon'(\infty)$], f_{Ri} and h_i are the dielectric strength, relaxation frequency (inverse of relaxation time) and distribution parameter ($0\leq hi\leq 1$) of the ith relaxation mode, respectively. $\varepsilon'(0)$ and $\varepsilon'(\infty)$ are the low and high frequency limiting values of the relative permittivity respectively. The third term of Eqs. (1) and (2) represents the contribution of electrode polarization capacitance at low frequencies with A and n as fitting parameters [4,13]. The term $\sigma/2\pi\varepsilon_0 f^k$ in Eqs. (1) and (3) accounts for the ionic conductance at low frequencies with k as fitting parameter [4,13]. In case of pure ohmic conductivity $k=1$. ε_0 ($=8.85$ pF/m) is the free space permittivity. The measured dielectric absorption (ε'') contains a contribution above 100 kHz due to finite resistance of the electrodes and lead inductance. An additional imaginary term $B\omega^m$ is empirically added in Eq. (1) to partially account for this effect [4,14,15], where B and m are fitting constants. The measured relative dielectric permittivity and dielectric loss data are separately fitted with Eqs. (2) and (3) by using a program developed with the Origin software and hence, the best fit values of various parameters of Eqs. (1)–(3) are obtained. Low and high frequency correction terms are calculated with the obtained parameters. These terms are then subtracted from the measured data to make it free from low and high frequency artifacts and thus, the corrected dielectric spectrum of ε' and ε'' could be obtained. The results of dielectric study have been reported for the gold coated cell since it gives the improved high frequency response of the dielectric spectrum.

3. Results and discussion

3.1. Thermodynamic and texture studies

As stated earlier, the racemic material is a mixture of R and S enantiomers in the ratio 1:1. Due to opposite optical handedness of these enantiomers, the chirality of the material and hence the net helicity vanishes. Fig. 1 shows the DSC thermogram for the heating and cooling cycles at the scanning rate of 10 K/min. The transition temperatures of various phases of the material and the corresponding transition enthalpies have been determined at different scanning rates varying from 1 to 10 K/min. The numbers 1 and 2 in Fig. 1 represent the two peaks of the Crystal (Cr) transition (melting point) indicating the polycrystalline behavior of the material. These two crystal phases are marked as Cr1 and Cr2 in Fig. 1. This phenomenon is observed in the cooling cycle also but the two peaks are not widely separated (shown by peak 7 in Fig. 1). The numbers 3 and 4 represent the transition peaks for the non chiral $\mathrm{SmC_A}$—SmC and SmC—Iso transitions, respectively in the heating cycle. The peaks 5–7 represent the Iso—SmC, SmC—$\mathrm{SmC_A}$ and $\mathrm{SmC_A}$—Cr phase transitions, respectively, for the cooling cycle. The expanded view of peaks 3 and 6 are shown in the insets of Fig. 1. The transition temperatures with varying scan rates in the heating and cooling cycles are plotted in Fig. 2. From Fig. 2, it can be seen that the transition temperatures of different phases vary linearly with scanning rate having opposite slopes in the